Repetitive load as a factor influencing mechanics of mesh implanted into abdominal wall. Experimental and numerical study.

Abstract

There are a number of papers discussing medical and mechanical aspects of ventral hernia management. Despite intensive work on the problem understanding, recurrences of the sickness still happen too often. For that reason new aspects of the problem must be considered. In this paper, a change in the abdominal implant's stiffness is discussed, which is caused by cyclic loading. Such loading influence abdominal implant e.g. while patient's coughing or exercising. For the first time this stiffness change is quantitatively described for a selected knitted mesh. The influence of mesh stiffness changes on repaired hernia persistence is studied. Then, *ex vivo* experiments on a repaired hernia model under cyclic pressure loading are performed. Finally, numerical simulations of the experiments are made in which stresses and forces in the system are calculated. The two following cases are considered. In the first case, the mesh has its baseline stiffness, and in the second case, the mesh is preconditioned by former loading; thus, it is stiffened. Reaction forces at the mesh fixation points appear to be approximately two-fold higher in the second case than in the first case. That may be a reason for a fixation damage in operated hernia system. The results presented shed new light on the necessary strength of mesh fixation in the abdominal wall. They enlarge the state of the art on laparoscopic hernia management with the use of a synthetic implant.

1. Introduction

Mesh placement has proven to be a superior method for hernia repair over suturing [1]. However, there is no consensus on the best way of treating a ventral hernia concerning the problems of pain and recurrence rate [2]. Reports on the hernia recurrence rate are very different. For some management schemes, the rate reaches 20%, as proven in [3]. Additionally,

[4] report a 20% recurrence rate for incisional hernia in United States as a result of suture or mesh device failure. On the other hand, according to [5], the failure rate of laparoscopic procedures is 1.2%, whereas according to [6], it is 4.4%. The variety of the rates obviously depends on the materials and the management scheme applied to a given medical case. Medical and engineering teams search for the most relevant hernia management via experiments on animals [7] [8], but there is no consensus concerning an experimental protocol [9]. Another approach is to analyse the problem via *ex vivo* experiments on repaired hernia models [10], [11], [12]. It is known that hernia repair fails when mesh fixation strength is insufficient[13]. The role of the mesh fasteners is to transmit loads between an implant and the abdominal wall. Sensitivity analysis of the reaction forces at the implant fixation points in a tissue-implant system is described in [14]. The following parameters are considered there: the mesh's initial tension, its initial deflection, fascia and mesh elasticity. It has been proven that the mesh elasticity is the most important factor, among others considered, that influences the force at the implant fasteners. Some researchers state that the best hernia operation outcome is obtained from mesh with elastic properties corresponding to the properties of the abdominal wall [15, 16]. The elastic properties of various meshes subjected to simple tension are studied in [17, 18, 19]. A review paper on that has been published recently [20]. The authors also discuss changes of the mechanical properties of implants subjected to cyclic loading tests [21, 22]. The repetitive loading of meshes in the abdominal cavity appears due to ever-changing intra-abdominal pressure. Experiments on selected meshes show that their elastic modulus approximately doubles due to repetitive loading in the physiological strain range [23,24].

In this paper, we discuss the influence of the mesh stiffness change caused by a repetitive intra-abdominal pressure load on the mesh-tissue junction force. The study is conducted on the example of a selected implant commonly used in hernia operations. DynaMesh®-IPOM (FEG Textiltechnik GmbH, Aachen, Germany) has been selected, which is a synthetic knit

mesh made of polypropylene and polyvinylidene fluoride. Two states of the material are distinguished based on the cyclic mesh loading: baseline and preconditioned. The mesh stiffness is identified for the two states. Experimental study of an operated hernia model's behaviour during repetitive pressure loading is performed. The forces at the mesh fixation points are calculated in numerical models validated to the experimental results.

The study extends the knowledge concerning operated hernia mechanics, which would contribute to improving mesh fixation design, which will result in the hernia recurrence rate declining and comfort of patients rising.

2. Materials and Methods

There are the following stages of the research: (i) identification of a constitutive model of the mesh in relation to its displacement states; (ii) *ex vivo* experiments on the mesh implanted into porcine abdominal wall subjected to cyclic pressure load; and (iii) numerical modelling of the experiments and force determination at the mesh fixation points.

2.1. Mesh material model relative to displacement states

A dense net model is selected for constitutive modelling of the implant. This model is suitable for textiles and technical fabrics, see, e.g.,[25]. It is shown, e.g., in [26], that this model can represent the DynaMesh material's behaviour. Two directions (1, 2) in the structure plane are distinguished in that model. It is assumed that stresses T in these two directions depend solely on the strains ε in these directions. The following constitutive equation is postulated [27]:

$$\begin{Bmatrix} T_1 \\ T_2 \end{Bmatrix} = \begin{bmatrix} F_1 & 0 \\ 0 & F_2 \end{bmatrix} \begin{Bmatrix} \varepsilon_1 \\ \varepsilon_2 \end{Bmatrix}, \tag{1}$$

in which F_1 and F_2 denote the material's tension stiffness in the two selected directions (1, 2). The stiffness functions are to be identified based on uniaxial mechanical tests, and thus, it is provided for DynaMesh. Rectangular samples of the mesh material have been subjected to

uniaxial tension tests on a Zwick Roell Z020 strength machine. The samples are cut out of one piece of a brand new just unpacked implant. As identified in the previous work [24], the implant material is considered to be orthotropic; thus, the material samples are cut in two perpendicular directions according to the specified orthogonality axes. Let the direction of highest material flexibility be denoted as '1' (longitudinal direction of an implant, determined by the knitting pattern) and let the perpendicular direction be denoted as '2'. The dimensions of the prepared strips are 120 × 30 mm. Such size allows for a clamp-to-clamp distance of 90 mm. With this setup, a uniaxial state is obtained in the central square of the sample, according to Saint Venant's principle. It is proved by [24] that the mesh reveals different stiffness when loaded in the physiological strain range for the first time than during subsequent loading. Based on that observation, two states of the material are distinguished, named the baseline and the preconditioned as introduced by [28] for soft tissues and addressed in [29]. The stiffness difference in both states results from residual displacements, which are 'remembered' by the mesh for a certain period of time after loading. The baseline state of the mesh is when its displacement field is zero before loading. The preconditioned mesh state is when its displacement field is non-zero before loading. The residual displacements observed may have two reasons: (1) structural, as in the knitted mesh the threads' weaves possibly tighten up, while the mesh is stretching, and (2) material because of the viscous properties of the mesh substance. It is shown in[24] that DynaMesh may restore its baseline state from the preconditioned one dependently on the load level applied.

The stiffness functions are identified based on simple tension tests (for the baseline material state) and based on cyclic loading tests (for the preconditioned material state). The identification is made by function fitting to experimental data sets within the optimisation process using the Marquardt–Levenberg variant of the least squares method [30]. The Sigma Plot program (Systat Software Inc., San Jose, USA) has been used, and the tolerance of the

fitting functions is assumed to be 1e-10. Engineering measures are used for stress T and strain ε.

- **Identification in the baseline state of the mesh**

The nonlinear experimental stress-strain curves obtained from simple tension tests are approximated by multilinear functions. Thus, piecewise constant stiffness functions are determined for the baseline material state for its two axes considered. Let the elastic modulus values, which describe these functions, be denoted as E_b.

- **Identification in the preconditioned state of the mesh**

The concept of stiffness function identification for the preconditioned state of the mesh is presented in the paper [24]. Here, the process is briefly described, and moreover, stiffness identification for strains not covered by the cyclic test is developed.

The stress-strain curves obtained from the cyclic loading tests have hysteretic characteristics, as presented in Fig. 1. Each cyclic experiment covers a different, but physiologic for abdominal wall, strain range. The strain ranges are determined based on [31]. On the other hand, the tests cover the force range possible for point fixation of the mesh made by tacks or sutures [13]. Four different cyclic tests have been performed for each considered orthogonality axis of the material.

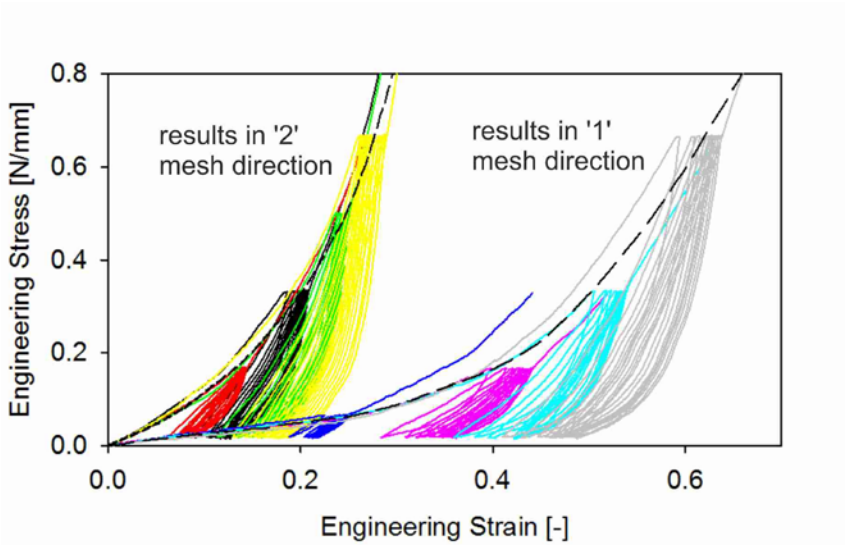

Fig. 1. Experimental stress–strain curves from simple tension tests (dashed lines) and cyclic tension (solid lines)

Elastic modulus values E_{pc} have been determined for the loading paths of each hysteresis by its local linear approximation (Fig. 2, step 1). A correlation coefficient of 0.99 is preserved in each curve fitting case. Based on that, the elastic modulus E_p of the material is determined for the strain range covered by a given cyclic experiment (Fig. 2, step 2). For each orthogonality axis of the mesh, four elastic modulus values are identified, as four different cyclic tests are performed (Fig. 2, step 3). To approximate elastic modulus values in strain ranges other than that covered by the cyclic experiments, a nonlinear stiffness function in the strain domain is fitted to the identified values (Fig. 2, step 4). The function to be fitted is taken from the uniaxial formulation of the Ogden model [32], as a stretch derivative of the stress:

$$T(\lambda) = \sum_{p=1}^{M} \mu_p \left(\lambda^{\alpha_p - 1} - \lambda^{-\frac{\alpha_p}{2} - 1} \right), \tag{2}$$

where $\lambda = 1 + \varepsilon$ denotes stretch, μ_p, α_p are parameters of the model and M is selected arbitrarily for the model to fit the data set well. The stiffness function $F(\lambda)$ is given as:

$$F(\lambda) = \frac{\partial T(\lambda)}{\partial \lambda} = \sum_{p=1}^{M} \mu_p \left[(\alpha_p - 1) \lambda^{\alpha_p - 2} + \left(\frac{\alpha_p}{2} + 1 \right) \lambda^{-\frac{\alpha_p}{2} - 2} \right] \quad . \tag{3}$$

To presume a continuous stress-strain curve for the material, the missing elastic modulus values are identified by local linear approximation of $T(\varepsilon)$ in the adequate strain ranges (Fig. 2, step 5). The $T(\varepsilon)$ function is determined from equation (2). The multilinear experimental $T(\varepsilon)$ function and piecewise constant $F(\varepsilon)$ (Fig. 2, step 6) are obtained finally for the material in the preconditioned state in that manner in both directions of the implant orthotropy.

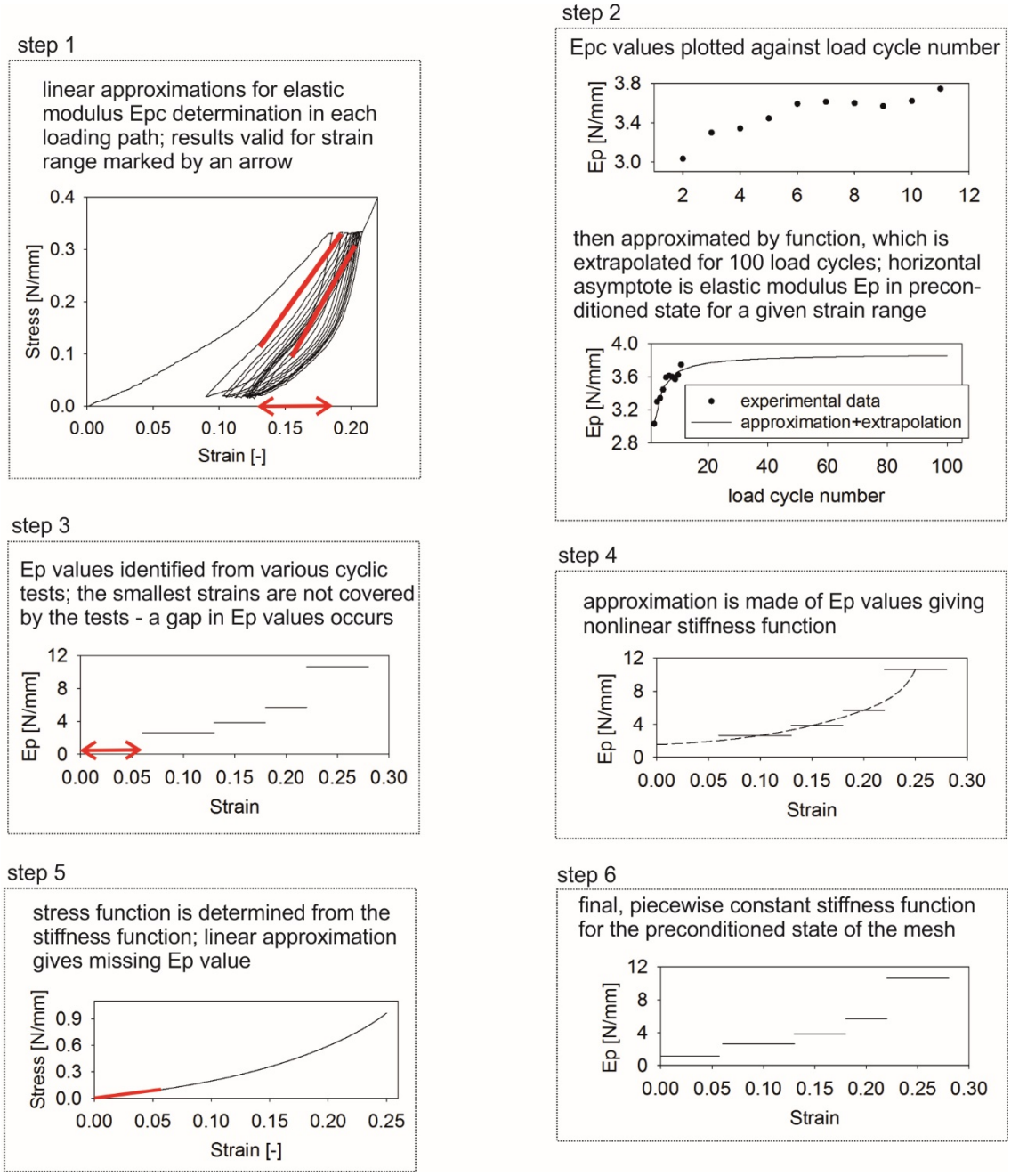

Fig. 2. Stiffness function identification procedure in the preconditioned material state

2.2. Experimental research on the mesh deflections under repetitive pressure loading

As it is difficult to observe mesh behaviour *in vivo* in patients, a special stand has been used in order to simulate the post-operative situation of the mesh implanted into an abdominal wall. The device allows for the operated hernia model to be loaded by pressure, which simulates intra-abdominal conditions [13]. The model used in this study is built of a porcine abdominal

wall in which a 7 cm wide hernia orifice is cut. The 'hernia' is then covered by DynaMesh® with a 5 cm overlap. The mesh is fixed by 19 trans-abdominal point sutures, regularly spaced. The diameter of the fixation circle is 13.5 cm. The model and the experimental stand are presented in Fig. 3. The model is loaded with a selected pressure value, which is kept for 2-3 minutes. Then, the model is relieved and stays unloaded for 10÷20 minutes. Different time periods of loading do not influence the displacement of the model, but different time periods of 'resting' (between loadings) allow for the viscous behaviour of the model to be observed. The first pressure applied to the model is 7.75 kPa. Then, the model is loaded with subsequent pressures of the following values: 3 kPa, 6 kPa, and 9 kPa, each applied four times in a row. The values correspond to pressures measured by [33] in the abdominal cavity. The following quantities are measured during the tests: pressure value, deflection of the mesh centre, deflection of a selected point of the 'hernia orifice' edge, and displacement of the fixation points in the plane of the model.

It is worth noting here that each load case is applied to a model of different geometry. Initially, before the first test, the model is flat (see Fig. 4a). After the first loading the model stays deflected, it gains a hat shape (see Fig. 4b), and starting from the second test, a hat-shaped model is loaded each time (Fig. 4c,d). In general, this shape has different heights before each test because of different time gaps between subsequent tests. That should simulate different time intervals in abdominal wall loading in real life. This hat shape is caused by residual displacements of the tissue and the mesh. The displaced state of the mesh makes it change its mechanical properties from baseline to preconditioned, as discussed before in a case of uni-axial mesh loading.

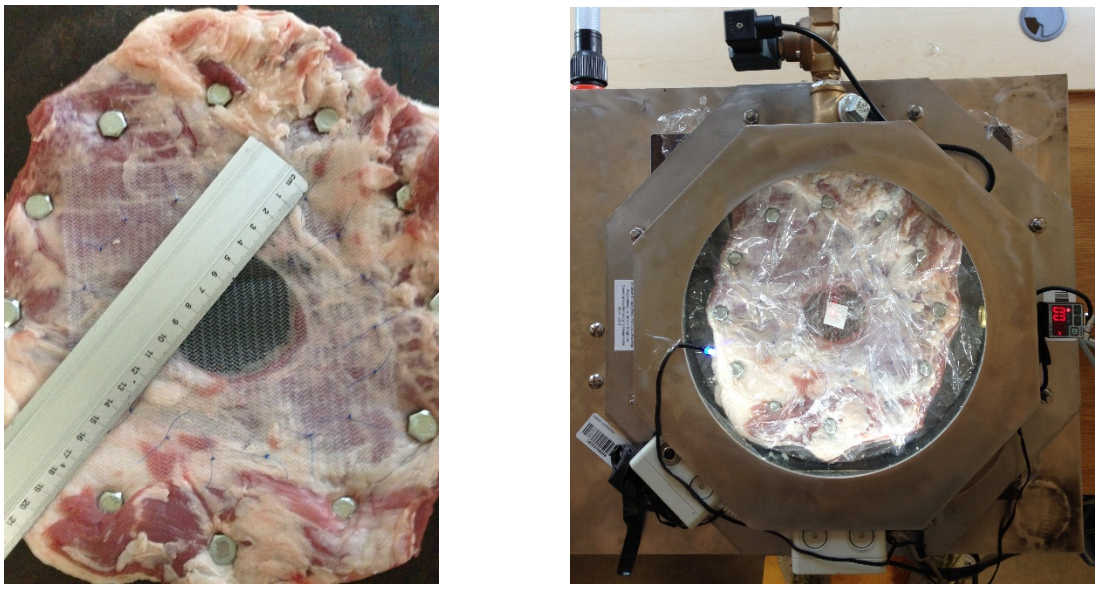

Fig. 3. (a) model of the operated hernia, (b) pressure chamber with the model inside

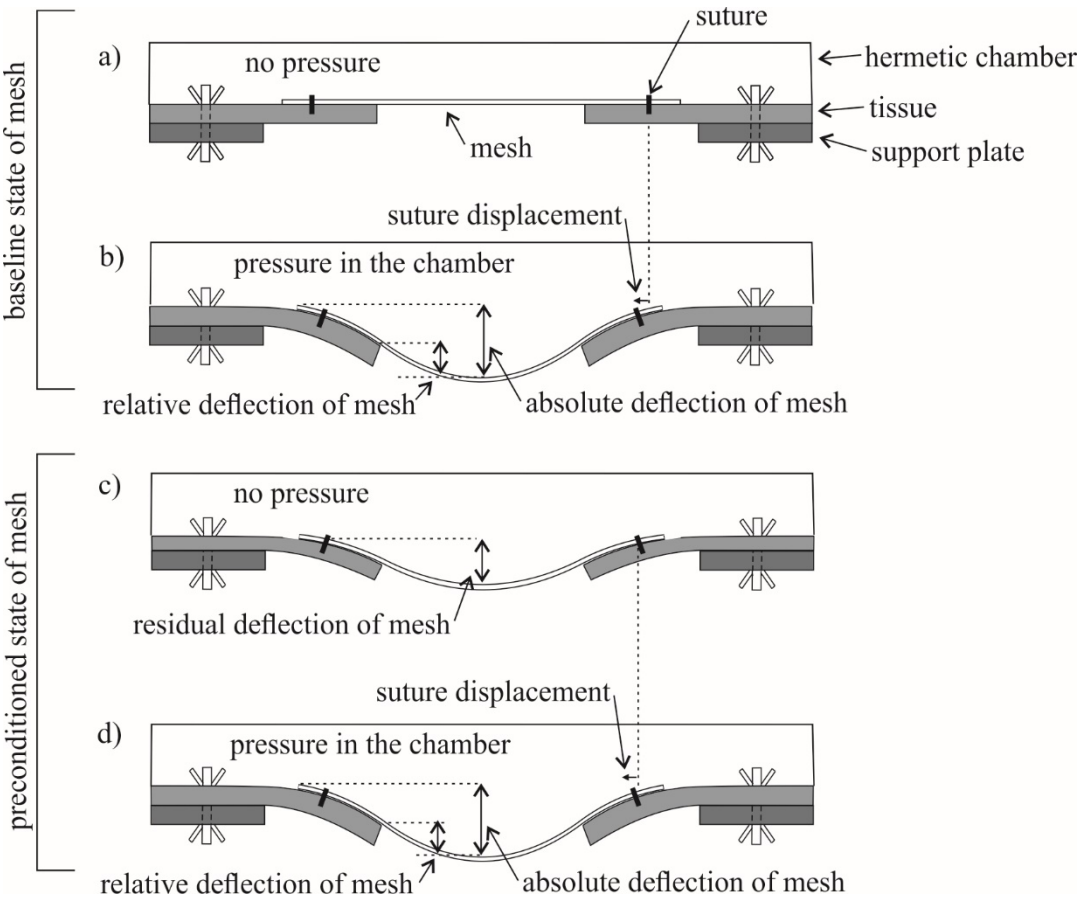

Fig. 4. Scheme of the experiment: a) before loading; b) first loading; c) after first loading; d) second loading

2.3. Numerical modelling of the experiments

To determine the forces at the mesh fixation points, a numerical model of the tested system has been built. The finite element method has been applied, and MSC.Marc commercial software has been used to simulate the model's mechanical behaviour. Two experimental cases are selected for numerical modelling: the first load case, in which the mesh is in its baseline state, and one of the subsequent load cases, when the mesh is in its preconditioned state. Thus, two geometries have been prepared for calculations.

In the calculations related to the baseline state of the mesh, the implant is described by a flat circular membrane supported on an elastic foundation representing the abdominal wall around the hernia orifice (Fig. 5). The 19 joints (sutures) in the physical model are represented here by nodes supported by elastic springs. Their stiffness corresponds to the stiffness of the connective tissue (see, e.g., [26]). Membrane finite elements with four nodes and three translational degrees of freedom in each node have been applied in the analysis. Orthotropic material defined within the dense net model with previously described stiffness functions has been used. The FEM model has been loaded according to the first experimental case where the pressure grows until the value of 7.75 kPa within 4 s. Then, the structure is unloaded.

In the preconditioned state, the model is similar, but it is hat-shaped in order to reflect the geometry with residual displacement of the mesh due to former loading. This hat shape is obtained by pre-loading of the flat model with the pressure giving the deformation expected as initial in the preconditioned state. The obtained geometry is then preserved, while the forces and stresses are released. The sixth experimental case is selected for simulations of the preconditioned mesh state. That is the first load case with pressure of 6 kPa (before that four load cases with pressure of 3 kPa were realised). Thus, the model is loaded with pressure growing until the level of 6 kPa within 4 s. After that, it is unloaded.

The FEM models with baseline and preconditioned mesh states are presented in Fig. 6. Besides the geometry, they also differ in the material properties, as two different stiffness functions are applied, as described in Section 2.1.

The model deformations and reaction forces at joints (membrane supports) have been calculated. Geometrical and material nonlinearities cause a stability problem in the static analysis of the membranes; thus, dynamic analysis has been performed with the parameters (load and time) reflecting the experiments made. Rayleigh damping parameters (mass damping coefficient α = 0.85 and stiffness damping coefficient β = 0.02) were applied according to a study [34] where the accuracy of the model and the convergence of the analysis were checked.

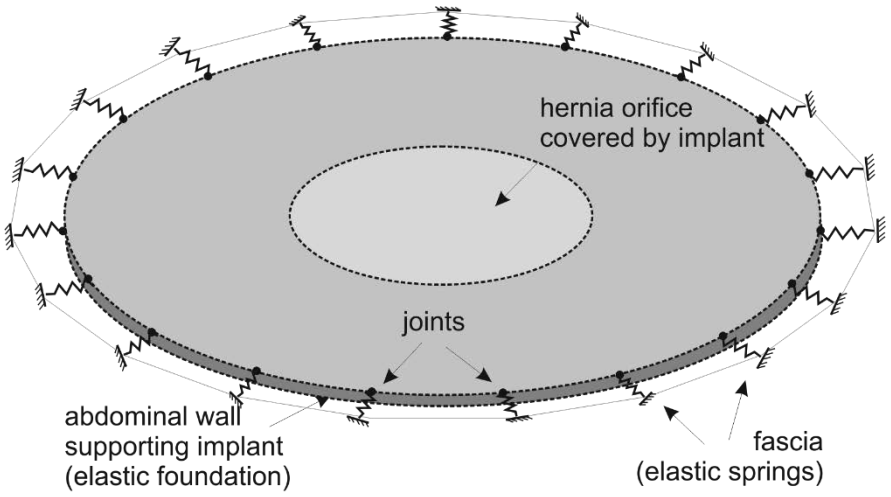

Fig. 5 Model of implanted surgical mesh

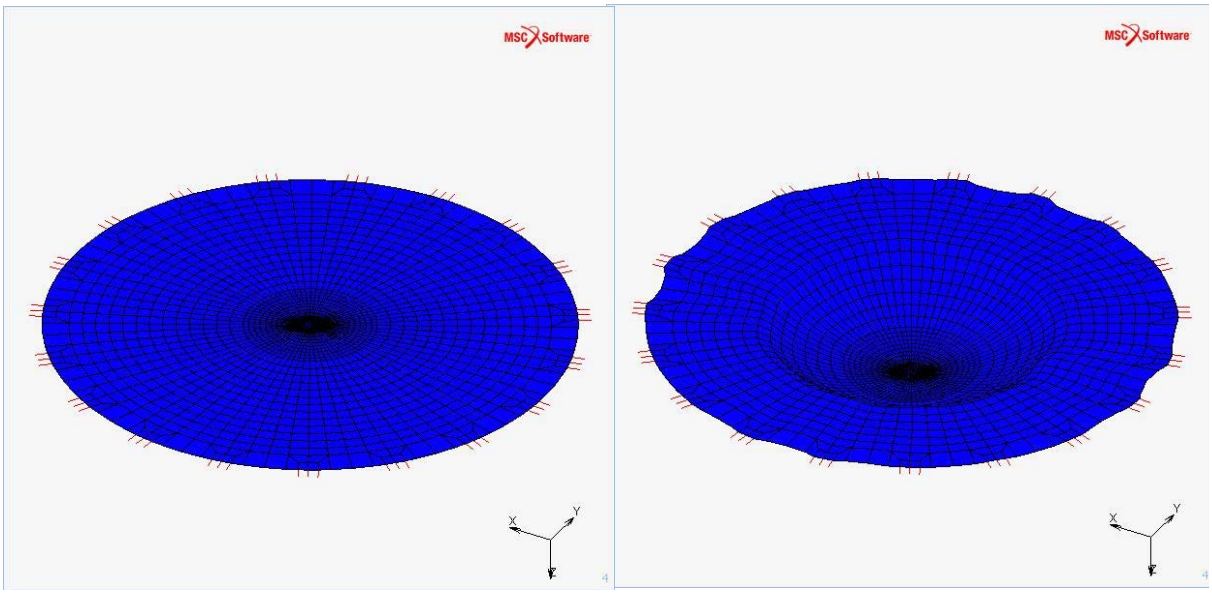

Fig. 6. Numerical model of the system: (a) flat model in the initial state of the mesh; (b) initially deformed model in the preconditioned state of the mesh

3. Results

- **The mesh stiffness functions relative to the displacement states**

In the baseline and preconditioned states of the mesh, the same strain ranges are selected for determination of the elastic modulus values. In Fig. 7, the elastic modulus values determined experimentally from cyclic tests are marked by coloured circles. Additionally, a nonlinear approximation of the stiffness function $F(\varepsilon)$ (see eq. (3)) is plotted. The parameters of this function are presented in Table 1. The elastic moduli identified additionally based on $F(\varepsilon)$ functions are marked on the graph by non-coloured circles. The values identified for the baseline state of the mesh are presented in the same graph for best comparison of the stiffness functions. Experimental stress-strain curves and their five (for the '1' axis of the mesh) or seven linear (for the other axis) representations for the two material states are presented in Fig. 8. For the preconditioned state, the stress-strain function is determined from Eq. (2) with

the parameters presented in Table 1. All values describing the piecewise constant stiffness functions of the material in two states in two orthogonal axes are presented in Table 2.

(a)

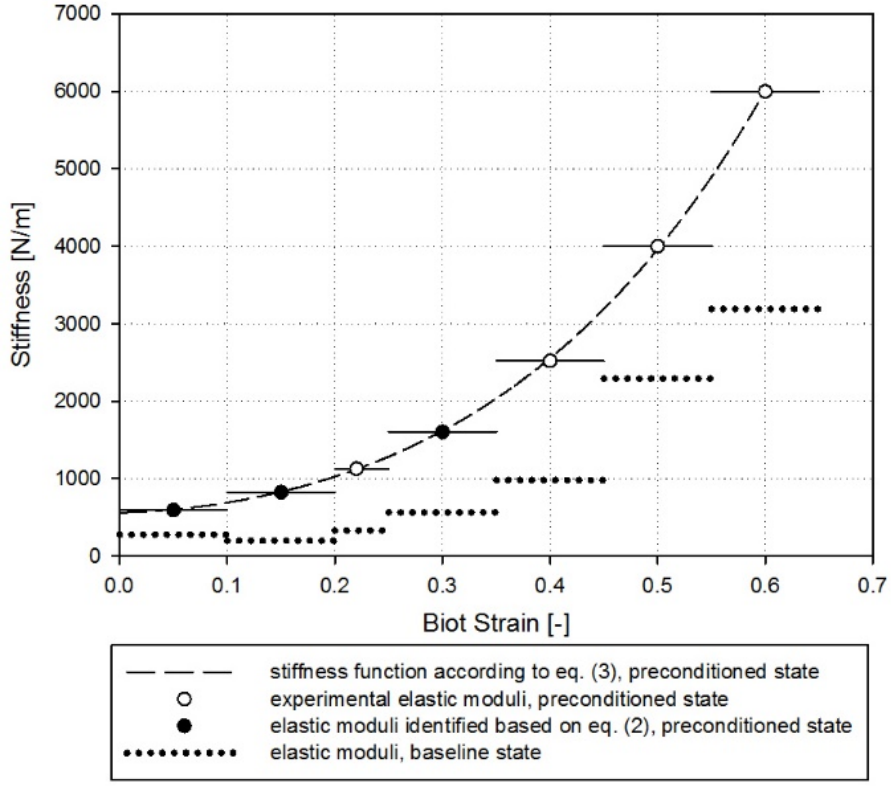

(b)

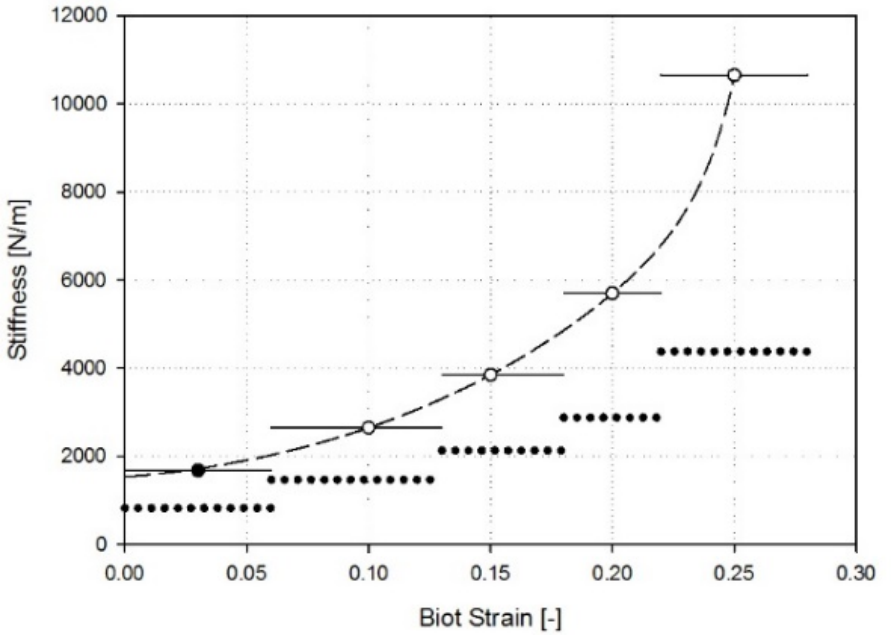

Fig. 7. Elastic moduli of DynaMesh in baseline and preconditioned displacement states in (a) ‘1’ axis, (b) ‘2’ axis of the mesh

(a)

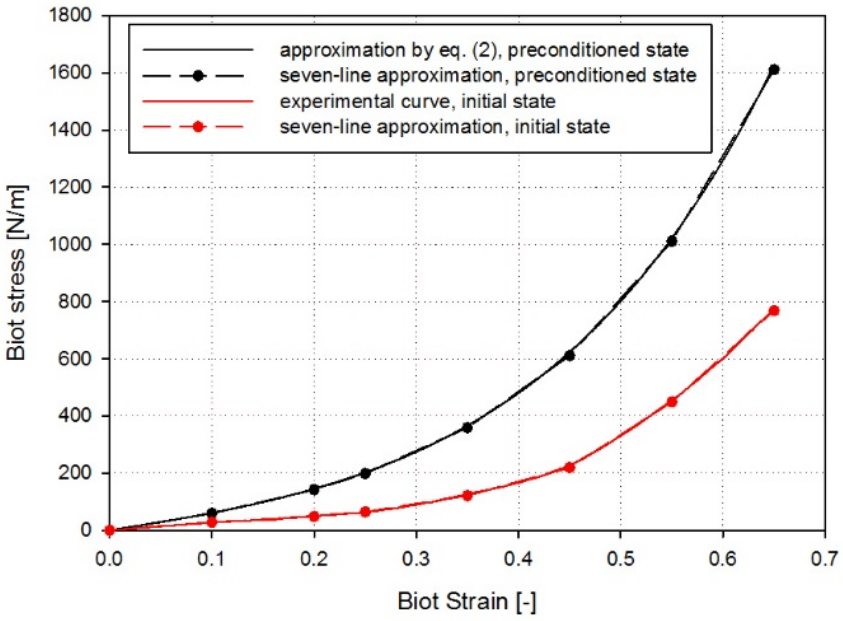

(b)

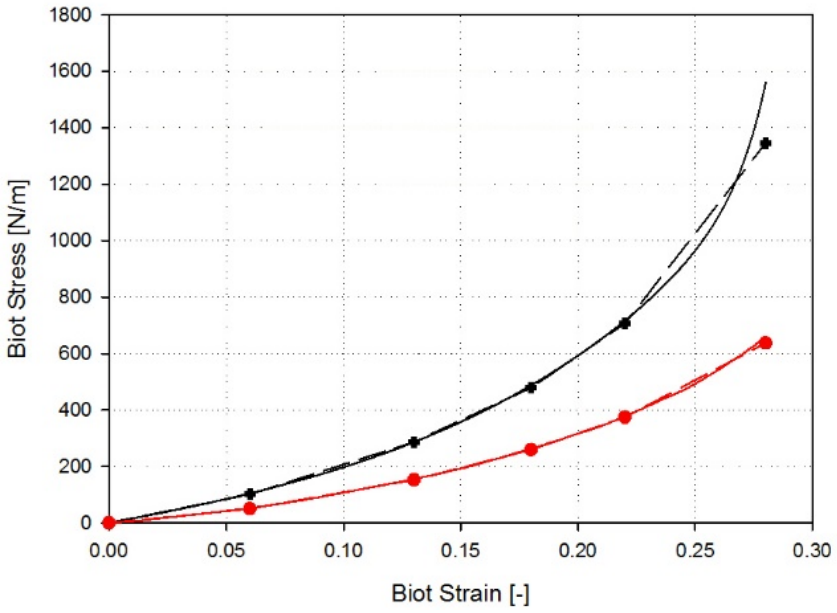

Fig. 8. Stress-strain relations for DynaMesh in the baseline state (experimental curve) and preconditioned state (approximated by Eq. (2) with parameters of stiffness curve fitting); (a) '1' axis, (b) '2' axis of the mesh.

Table 1. Parameters of the stiffness functions fitted to the experimental elastic moduli identified in the preconditioned state of the mesh.

Mesh axis	Parameters of the fitted function (3)			
	μ_1 [N/m]	μ_2 [N/m]	α_1	α_2
'1'	36.8	23.2e3	8.53	0.00260
'2'	1.33e-9	87.1	107	11.7

Table 2. Elastic modulus values in N/m for different strain ranges and two axes of the mesh; E_b is in baseline mesh state and E_p is for preconditioned state

'1' axis of the mesh							
Strain ranges	0-0.1	0.1-0.2	0.2-0.25	0.25-0.35	0.35-0.45	0.45-0.55	0.55-0.65
E_b	280	200	330	566	983	2290	3190
E_p	594	824	1130	1600	2520	4000	6000

'2' axis of the mesh					
Strain ranges	0-0.06	0.06-0.13	0.13-0.18	0.18-0.22	0.22-0.28
E_b	825	1470	2130	2880	4380
E_p	1680	2650	3850	5700	10650

- **Experiments on mesh deflection under repetitive pressure load**

The model deflections are of major interest in experimental study. They serve as the state variables in numerical model validation. The first load of the system is realised by the pressure of 7.75 kPa, and the absolute mesh deflection (see Fig. 4) is 31.5 mm, with the initial value equal to zero. As mentioned in Section 2.2, the model reveals residual deflection after

each pressure loading. This deflection slowly reduces within time in the unloaded part of the experiment. The model was flat again within 12 hours after the experiment.

An interesting observation is that the mesh absolute deflection is the same for repeatable pressure of the same value, independently of the different levels of residual deflection before loading. This has been observed by preserving different gap times between successive loadings. The following values of absolute deflection for the applied pressure levels have been measured: 28 mm for 3 kPa (with initial absolute mesh deflection in a range of 12 – 15 mm); 32 mm for 6 kPa (with initial values in a range of 15 – 19 mm); and 34.5 mm for 9 kPa (with initial values in a range of 16.5 – 20.5 mm).

The detailed results of the experiments selected for numerical modelling are presented in Table 3.

- **Numerical results**

During the analysis of both baseline and preconditioned states of the implant, the forces at the joints are calculated (tangential to the model). These forces are the key factors ensuring hernia repair persistence [13]. Due to the anisotropic material properties, different reactions are obtained in different radial directions of the model. The maximal forces are obtained in the direction of the highest stiffness of the implant. They take the following values: 0.870 N in the baseline state and 1.42 N in preconditioned state of the implant. The membrane deflection in both cases has been approximately 30 mm (see Table 3). The maximum principal stress distribution in the material in the two states is presented in Fig. 9.

Table 3. Experimental and numerical displacements in the models; absolute and relative displacement is marked in Fig. 4.

State of mesh		Baseline		Preconditioned	
Result type		experimental	numerical	experimental	numerical
Pressure [kPa]		7.75	7.75	6.00	6.00
Initial mesh deflection (before loading) [mm]	Absolute	0	0	15.0	15.1
	Relative	0	0	9.80	12.7
Mesh deflection under pressure [mm]	Absolute	31.5	32.3	32.0	31.1
	Relative	17.2	20.6	17.7	20.9
Suture displacement in radial direction [mm]	Along ‘1’ axis of mesh	1.90	0.270	0.970	0.120
	Along ‘2’ axis of mesh	2.80	1.02	2.10	0.510

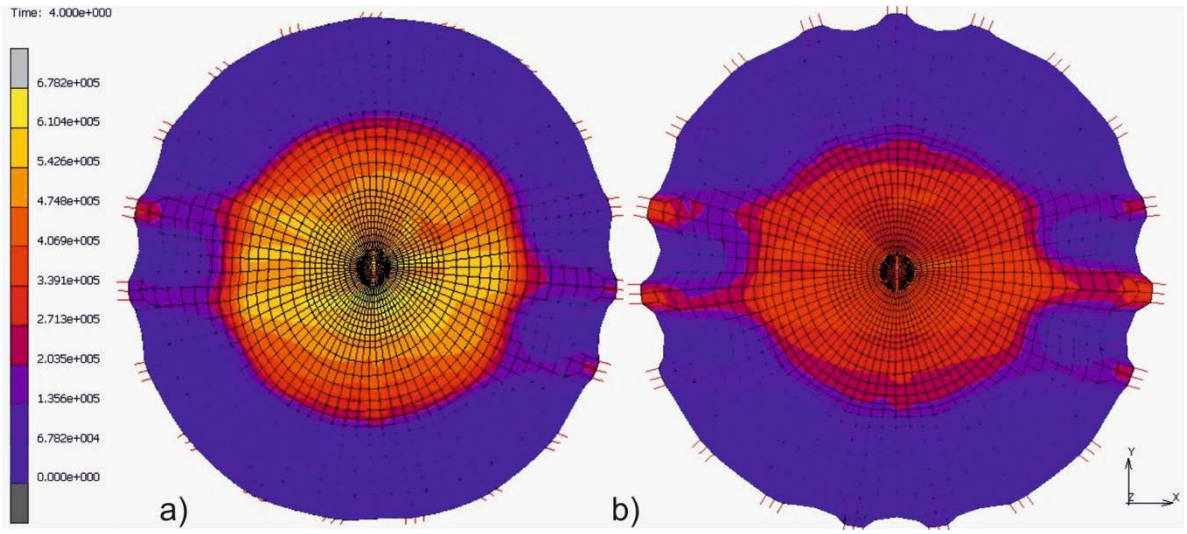

Fig. 9. Maximum principal stress distribution [Pa] in implant subjected to intra-abdominal pressure: (a) baseline properties of implant, (b) preconditioned state of implant

Discussion

In this study, experiments on implant material in 1D and 3D tensile states are described. They prove that the mechanical behaviour and parameters of the studied implant are dependent on load history. Subsequently, forces that appear at the implant fixation points in the abdominal wall due to intra-abdominal pressure depend on load history as well. On the selected example implant, commonly used in hernia operations, quantitative differences between reaction forces are noted for the implant being in different displacement states. It is proposed to distinguish two material states, baseline and preconditioned, and to determine stiffness functions for the material being in the two states based on simple and cyclic tension tests.

The material's behaviour is nonlinear, but one can observe an approximate twofold increase of elastic modulus when the material is reloaded. That is visible in both directions of the material orthotropy (see Fig. 7). The stiffness functions identified for the implant are applied in numerical simulations of an operated hernia model. One model is built for the baseline implant state, and another for its preconditioned state. The calculated maximum reaction forces in the two models differ by 60%; changing of the mesh state from baseline to preconditioned causes the junction force to rise.

The question is what junction forces appear in real abdominal wall with an operated hernia? Practice shows that overloaded joints may break and cause recurrence of the hernia. The reason may involve underestimation of the necessary fixation strength for a given mesh. It is known from previous works (e.g., [14]) that the stiffer the mesh is, the bigger the junction force is at the fixation points. Therefore, the stiffening effect of the mesh due to reloading should be considered in assessments of necessary fixation strength. Still, there are increasing data, which may help in calculations concerning the reliability of different surgical solutions.

Another question is if the mesh can recover its baseline state from the preconditioned? Our 1D and 3D experiments show that it can, but the question if that is possible in living

conditions is open. For that reason, the more secure approach in calculations is to include the preconditioned mesh state.

The presented 3D numerical simulations show another interesting feature of the considered implant. When its baseline stiffness is considered, the maximum stress in the structure is concentrated in its central part, in the region of the hernia orifice. However, when the preconditioned material state is considered, the maximum stress is more concentrated along a stripe-like area indicating the stiffer direction of the implant. In such a case, the circular implant may rather work like a tendon and then stress is concentrated along it, which causes a considerable junction force increase in that direction. That is certainly due to orthotropic properties of the implant, which change due to reloading. Such results may also be valid for other implants, as a significant majority of them have orthotropic properties; that is desirable because of the orthotropy of the abdominal wall itself.

The parameters of the experiments made in this study correspond to the real working conditions of implanted mesh. First, tensile tests are performed in a load bearing capacity range typically used in joints and in the strain range of abdominal wall. Second, simple tension and cyclic tension are possible states for abdominal wall. Third, the pressure applied in 3D experiments is realised by air, which is a more realistic simulation than, e.g., a ball burst; air pressure does not influence the deformation shape of the model. Pressure loading is also used in other studies [10, 11].

Conclusions

The results prove that the reaction forces calculated at the mesh fixation points increase significantly when the mesh state changes from the initial to the preconditioned, which results from different material characterisation of the same implant when working in the pre-deformed state after initial loading. That important finding proves the necessity of considering

the stiffening effect in the fixation planning for a certain surgical mesh before the hernia repair.

If the mesh displacement state is not considered in the fixation planning, it is possible that the fixation strength will be underestimated, and it can fail more easily. Taking into account the recurrence rate of ventral hernias discussed in the Introduction, such a scenario may occur in practise.

Limitations of the study

According to doctors, most recurrences occur shortly after the operation, when the mesh is not yet incorporated with fascia. Our research is devoted to such a situation, so no tissue overgrowth is considered here.

There is no contact between tissue and implant defined in the numerical model, and the abdominal wall supporting the mesh is included in the model as an elastic foundation of the membrane implant. Additionally, the abdominal wall anisotropy is omitted in the model.

The research is conducted for one kind of mesh, but the stiffening effect is stated also for other knitted implants, e.g., [23, 22].

As the residual displacements of the mesh vanish within 12 hours after the tests, the material's behaviour can be generally considered viscous, which will be the next stage of the study. That will allow for residual stresses to also be considered in the preconditioned model besides residual displacements.

Acknowledgements

Calculations have been carried out at the Academic Computer Centre in Gdańsk.

References

1. Burger, J. *et al.* Long-term follow-up of a randomized controlled trial of suture versus mesh repair of incisional hernia. *Ann. Surg.* **240,** 578–585 (2004).

2. Pawlak, M., Bury, K. & Śmietański, M. The management of abdominal wall hernias - in search of consensus. *Wideochirurgia i inne Tech. małoinwazyjne = Videosurgery other miniinvasive Tech. / Kwart. Pod patronatem Sekc. Wideochirurgii TChP oraz Sekc. Chir. Bariatrycznej TChP* **10,** 49–56 (2015).

3. Pawlak, M. *et al.* Comparison of two different concepts of mesh and fixation technique in laparoscopic ventral hernia repair: a randomized controlled trial. *Surg. Endosc.* (2015). doi:10.1007/s00464-015-4329-0

4. Ibrahim, M. M. *et al.* Modifying Hernia Mesh Design to Improve Device Mechanical Performance and Promote Tension-Free Repair. *J. Biomech.* (2018). doi:10.1016/j.jbiomech.2018.01.022

5. Sauerland, S., Walgenbach, M., Habermalz, B., Cm, S. & Miserez, M. Laparoscopic versus open surgical techniques for ventral or incisional hernia repair (Review). *Cochrane Libr.* (2011).

6. Bansal, V. K. *et al.* A prospective randomized study comparing suture mesh fixation versus tacker mesh fixation for laparoscopic repair of incisional and ventral hernias. *Surg. Endosc.* **25,** 1431–8 (2011).

7. Konerding, M. a, Chantereau, P., Delventhal, V., Holste, J.-L. & Ackermann, M. Biomechanical and histological evaluation of abdominal wall compliance with intraperitoneal onlay mesh implants in rabbits: a comparison of six different state-of-the-art meshes. *Med. Eng. Phys.* **34,** 806–16 (2012).

8. Anurov, M. V, Titkova, S. M. & Oettinger, a P. Biomechanical compatibility of surgical mesh and fascia being reinforced: dependence of experimental hernia defect repair results on anisotropic surgical mesh positioning. *Hernia* **16,** 199–210 (2012).

9. Vogels, R. & Kaufmann, R. Critical overview of all available animal models for abdominal wall hernia research. *Hernia* (2017). doi:10.1007/s10029-017-1605-z

10. Kallinowski, F. *et al.* Dynamic intermittent strain can rapidly impair ventral hernia repair. *J. Biomech.* (2015). doi:10.1016/j.jbiomech.2015.09.045

11. Lyons, M., Mohan, H., Winter, D. C. & Simms, C. K. Biomechanical abdominal wall model applied to hernia repair. *Br. J. Surg.* **102,** e133–9 (2015).

12. Guérin, G. & Turquier, F. Impact of the defect size, the mesh overlap and the fixation depth on ventral hernia repairs: a combined experimental and numerical approach. *Hernia* **17,** 647–55 (2013).

13. Tomaszewska, A. *et al.* Physical and mathematical modelling of implant-fascia system in order to improve laparoscopic repair of ventral hernia. *Clin. Biomech. (Bristol, Avon)* **28,** 743–51 (2013).

14. Szymczak, C., Lubowiecka, I., Tomaszewska, A. & Śmietański, M. Modeling of the fascia-mesh system and sensitivity analysis of a junction force after a laparascopic ventral hernia repair. *J. Thoretical Appl. Mech.* **48,** 933–950 (2010).

15. Junge, K. *et al.* Elasticity of the anterior abdominal wall and impact for reparation of incisional hernias using mesh implants. *Hernia* **5,** 113–118 (2001).

16. Song, C., Alijani, A., Frank, T., Hanna, G. & Cuschieri, A. Elasticity of the living abdominal wall in laparoscopic surgery. *J. Biomech.* **39,** 587–91 (2006).

17. Saberski, E. R., Orenstein, S. B. & Novitsky, Y. W. Anisotropic evaluation of synthetic surgical meshes. *Hernia* **15,** 47–52 (2011).

18. Hernández-Gascón, B. *et al.* Mechanical behaviour of synthetic surgical meshes: finite element simulation of the herniated abdominal wall. *Acta Biomater.* **7,** 3905–13 (2011).

19. Ciritsis, A., Horbach, A., Staat, M., Kuhl, C. K. & Kraemer, N. A. Porosity and tissue integration of elastic mesh implants evaluated in vitro and in vivo. 1–7 (2017). doi:10.1002/jbm.b.33877

20. Deeken, C. R. & Lake, S. P. Mechanical properties of the abdominal wall and biomaterials utilized for hernia repair. *J. Mech. Behav. Biomed. Mater.* **74,** 411–427 (2017).

21. Eliason, B. J., Frisella, M. M., Matthews, B. D. & Deeken, C. R. Effect of repetitive loading on the mechanical properties of synthetic hernia repair materials. *J. Am. Coll. Surg.* **213,** 430–5 (2011).

22. Velayudhan, S., Martin, D. & Cooper-White, J. Evaluation of dynamic creep properties of surgical mesh prostheses--uniaxial fatigue. *J. Biomed. Mater. Res. B. Appl. Biomater.* **91,** 287–96 (2009).

23. Li, X. *et al.* Characterizing the ex vivo mechanical properties of synthetic polypropylene surgical mesh. *J. Mech. Behav. Biomed. Mater.* **37,** 48–55 (2014).

24. Tomaszewska, A. Mechanical behaviour of knit synthetic mesh used in hernia surgery. *Acta Bioeng. Biomech.* (2016). doi:10.5277/ABB-00185-2014-03

25. Ambroziak, A. & Klosowski, P. Review of constitutive models for technical woven fabrics in finite element analysis. *AATCC Rev.* **11,** 58–67 (2011).

26. Lubowiecka, I. Behaviour of orthotropic surgical implant in hernia repair due to the material orientation and abdomen surface deformation. *Comput. Methods Biomech. Bomedical Eng.* **18,** 223–32 (2015).

27. Branicki, C. & Kłosowski, P. Statical analysis of hanging textile membranes in nonlinear approach. *Arch. Civ. Eng.* **XXIX,** 189–219 (1983).

28. Fung, Y. C. *Biomechanics. Mechanical Properties of Living Tissues*. 1–568 (Springer-Verlag New York, Inc., 1993).

29. Maurer, M. M., Röhrnbauer, B., Feola, a, Deprest, J. & Mazza, E. Mechanical biocompatibility of prosthetic meshes: A comprehensive protocol for mechanical characterization. *J. Mech. Behav. Biomed. Mater.* **40,** 42–58 (2014).

30. Brandt, S. *Statistical and Computational Methods in Data Analysis (Ed. 3)*. (Springer Verlag, 1997).

31. Szymczak, C., Lubowiecka, I., Tomaszewska, A. & Smietański, M. Investigation of abdomen surface deformation due to life excitation: implications for implant selection and orientation in laparoscopic ventral hernia repair. *Clin. Biomech. (Bristol, Avon)* **27,** 105–10 (2012).

32. Ogden, R. W. *Non-linear elastic deformations*. 1–526 (Dover Publications, Inc., 1997).

33. Cobb, W. S. *et al.* Normal intraabdominal pressure in healthy adults. *J. Surg. Res.* **129,** 231–5 (2005).

34. Lubowiecka, I. Mathematical modelling of implant in an operated hernia for estimation of the repair persistence. *Comput. Methods Biomech. Biomed. Engin.* **18,** (2015).